A New Polystyrene-Polyvinyl Pyridinium Ionic Copolymer Dopant for N-Type All-Polymer Thermoelectrics with High Stable Conductivity Relative to Seebeck Coefficient Giving High Power Factor

Jinfeng Han[1], Emma Tiernan[2], Taein Lee[1], Arlene Chiu[3], Patty McGuiggan[1], Nicholas Adams[1], John A. Tomko[2], Patrick E. Hopkins[2,4,5], Susanna M. Thon[3], John D. Tovar[1], Howard E. Katz[1,]*

[1]Department of Materials Science and Engineering and Department of Chemistry, Johns Hopkins University, 3400 North Charles Street, Baltimore, Maryland 21218, United States

[2]Department of Mechanical and Aerospace Engineering, University of Virginia, Charlottesville, VA 22904, United States

[3]Department of Electrical and Computer Engineering, Johns Hopkins University, 3400 North Charles Street, Baltimore, Maryland 21218, United States

[4]Department of Materials Science and Engineering, University of Virginia, Charlottesville, VA 22904, United States

[5]Department of Physics, University of Virginia, Charlottesville, VA 22904, United States

Keywords: n-type polymer dopant, electrical conductivity, Seebeck coefficient, all-polymer thermoelectric, electron mobility

Abstract: A novel n-type copolymer dopant polystyrene-polyvinyl hexylpyridinium fluoride (PSpF) with fluoride anion is designed and synthesized by reversible addition-fragmentation chain transfer (RAFT) polymerization. To our knowledge, it is the first polymeric fluoride dopant. Electrical conductivity of 4.2 S cm^{-1} and high power factor of 67 μW m^{-1} K^{-2} are

achieved for PSpF doped polymer films, with a corresponding decrease in thermal conductivity as the PSpF concentration is increased, giving the highest *ZT* of 0.1. An especially high electrical conductivity of 58 S cm^{-1} at 88 ℃ and outstanding thermal stability were recorded. Further, organic transistors of PSpF-doped thin films exhibit high electron mobility and Hall mobility of 0.86 and 1.70 $cm^2 V^{-1} s^{-1}$, respectively. The results suggest that polystyrene-polyvinyl pyridinium salt copolymers with fluoride anion are promising for high performance n-type all-polymer thermoelectrics. This work provides a new way to realize organic thermoelectrics with high conductivity relative to Seebeck coefficient, high power factor, thermal stability and broad processing window.

N-doping has been employed as a crucial process for organic transistors,[1] solar cells,[2] organic light-emitting diodes[3] and photocatalysts.[4] Recently, n-doping for use in organic thermoelectrics (OTEs) was studied extensively to control carrier density and electrical conductivity.[5] Organic thermoelectrics can enable emergent applications in large area and flexible/wearable green energy-harvesting devices, which can convert the heat from the human body into electricity.[6] Power factor (*PF*, see below) is commonly used for evaluating the performance of organic thermoelectrics. For example dilute sulfuric acid-treated poly(3,4-ethylenedioxythiophene):poly(4-styrenesulfonate) (PEDOT:PSS) exhibits high electrical conductivity ≥ 3000 S cm^{-1}, that can equal to or exceed that of indium tin oxide (ITO) or metal electrodes.[7] Benefitting from high electrical conductivity, PEDOT:PSS has also been used as a hole-transporting interface material and as electrodes for organic solar cells.[8] N-type doping results in much lower σ than p-doping with most σ less than 1 S cm^{-1},[9] and usually uses small molecule n-dopants, such as 4-(1,3-dimethyl-2,3-dihydro-1H-benzoimidazol-2-yl)phenyl)dimethylamine (N-DMBI), tetrakis(dimethylamino)ethylene (TDAE), tetra-n-butylammonium fluoride (TBAF) and a polycyclic triaminomethane (TAM) donor.[5b, 10] To improve the doping efficiency and electrical conductivity, Han Guo et al.

reported the air-stable precursor-type molecular dopants for high doping efficiency with a very short doping time of 10 s.[11]

Recently, most attention was focused on the design and synthesis of novel n-type conjugated polymers. The Lei group reported a new polymer P(PzDPP-2FT) with a zigzag backbone doped with $CoCp_2$ showing a high electrical conductivity over 120 S cm^{-1}.[12] The acceptor-acceptor polymer with electron-deficient double B←N bridged bipyridine unit was proved to be an excellent organic thermoelectric material.[13] In addition, high electrical conductivity of organic thermoelectrics based on N-DMBI and similar dopants can only be achieved from narrow and limited dopant concentrations.[14] For example, FBDPPV doped by N-DMBI exhibits a high electrical conductivity of 12 S cm^{-1}.[15] Recently, many new BDOPV-based polymers were reported for n-type thermoelectrics with conductivity over 10 S cm^{-1}. However, conductivity over 1 S cm^{-1} was only achieved between N-DMBI concentration of 3 and 15 wt%. The thermoelectric performance of polymers is usually evaluated by *ZT* and power factor (*PF*):

$$ZT = \frac{S^2 \sigma T}{\kappa} \qquad (1)$$

$$PF = S^2 \sigma \qquad (2)$$

in which, *S* is Seebeck coefficient, σ is electrical conductivity, *T* is absolute temperature, and κ is thermal conductivity.[16] Currently, the common way to enhance the thermoelectric efficiency of polymers is increasing the *S* and σ,[17] because conjugated polymers usually show similar κ.[18] Though the κ of conjugated polymers is much lower than those of electrically conductive inorganic materials,[18a] it's still can be decreased to enhance the *ZT*. Polystyrene (PS) usually presents much lower thermal conductivity (0.03-0.18 W m^{-1} K^{-1})[19] than the conjugated polymers (0.3-0.5 W m^{-1} K^{-1})[20], so it can be useful to decrease thermal conductivity while increasing electrical conductivity by introducing polystyrene into dopants.

Compared with small molecule dopants, polymer dopants doped films can achieve higher stability and considerable electrical conductivity. Keli Fabiana Seidel et al.[21] and Chi-Yuan Yang et al.[22] reported the polymer dopant poly(ethyleneimine) (PEI) doped P(NDI2OD-T2) and poly(benzimidazobenzophenanthroline) (BBL) with σ of 0.002 and 8 S cm^{-1}, respectively. Kai Xu et al. reported the conjugated polymer dopants (P(g42T-T)) and (P(g42T-TT)) which doped the ladder polymer BBL at a heterojunction with excellent thermal stability.[23] To our knowledge, polystyrene-based polymeric fluoride (or other anionic salt) n-type dopants for n-type conjugated polymers, structurally analogous to PSS for PEDOT, have not yet reported. PSS is a PS derivative with a sulfonic acid group, which makes it an ionic polymer.[24] Previously, TBAF[1, 25] and the Meisenheimer complexes NDI-TBAF[26] containing ammonium cation (N^+) and F anion (F^-) were proved to be effective n-type dopants for conjugated polymers. The chemical structure of PSS inspired us to combine PS and the ions of N^+ and F^- for design and synthesis of a polymeric n-type dopant. Pyridine has a similar chemical structure to benzene, and can react with halohydrocarbon to achieve N^+.[27] The copolymer dopant PSpF can enhance n-doping ability and maintain the ambient stability of PS. The n-type conjugated polymer PFClTVT (**Figure 1**) presents excellent n-doping performance with N-DMBI which is similar with other BDOPV-based n-type polymers;[28] here we use it to dope with PSpF for n-type organic thermoelectrics. The highest σ of 4.2 S cm^{-1} and *PF* of 60 μW m^{-1} K^{-2} are achieved at room temperature, and high σ of 58 S cm^{-1} was detected at 88 ℃.

The polystyrene-polyvinyl pyridine (PS-P) copolymer with 5 mol% pyridine rings was synthesized by RAFT living radical polymerization with molecular weight of 334 kDa.[29] The copolymer PSpBr containing Br - was achieved by nucleophilic substitution with bromohexane (supporting information). A PS-P-based polymer dopant PSpF was obtained

from PSpBr by ion exchange reaction (**Figure 1a**). The absorption spectra of PSpF in solution are shown in **Figure 1b**; two absorption peaks were detected at 294 and 440 nm, respectively. They can be attributed to the absorption of polystyrene[30] and fluoride polypyridine salt, respectively.[31] The PSpF film had three absorption peaks at 224, 260 and 431 nm, respectively; the blue shifts of 34 and 9 nm were observed in the absorption of polystyrene and polypyridine salt, respectively. The differential scanning calorimeter (DSC) traces of polymer PS-P and PSpF were measured under N_2 between 40 and 250 ℃. The glass transition temperatures (T_g) of PS-P and PSpF are 114 and 109 ℃, respectively. The relatively lower T_g of PSpF is related to the hexyl sidechains on pyridine. The unit "wt %" in this paper means weight ratio of PSpF compared to the conjugated polymer PFClTVT, for example, 100 wt % means equal weights of conjugated polymer and PSpF.

The UV-vis-NIR absorption spectra of pristine and doped PFClTVT films are shown in **Figure 2a** and S5b. The pristine film displays two absorptions peaks at 465 and 777 nm, which can be attributed to π-π* transition and intramolecular charge transfer.[32] With 5 wt% PSpF doping, stronger absorption was detected in the low energy region of 1000-1800 nm (**Figure 2b**), contributed by polaron/bipolaron transitions[33] and similar to N-DMBI doped films.[34] However, the absorption of neutral N-DMBI doped films is usually bleached,[28a] here the absorption intensity increases with PSpF doping, different from N-DMBI-doped films. When the weight fraction of PSpF increases to 30 wt%, absorption in the low energy region is much stronger and two new weak absorption peaks at 1350 and 1596 nm appear (**Figure 2b**). With the weight fraction of PSpF increasing from 30 to 75 wt%, the two peaks become stronger and the neutral absorption in the high energy region becomes weaker but is still stronger than for pristine PFClTVT. The absorption result demonstrates that effective doping occurs in films of PFClTVT: PSpF. The electron paramagnetic resonance (EPR) spectra of pristine and doped PFClTVT solution are shown in **Figure 2c**. There is no radical

peak for pristine PFClTVT solution, while an obvious radical peak was detected in 5 wt% PSpF doped solution that is at the similar magnetic field with N-DMBI doped polymers.[28a, 35] When PSpF fraction increases to 50 and 100 wt%, the EPR intensity is much stronger than 5 wt% PSpF doped solution, and further proves the effective doping by PSpF. The absorption in the region of 1300-1800 nm (near IR, referenced to absorbance at 1200 nm) increases when the doping ratio increases from 5 wt% to 75 wt%, fully as expected, and then decreases when the dopant/polymer ratio is 100 wt%. The EPR spectra are consistent with near IR absorption spectra results. The EPR intensity increases when the dopant ratio increases from 5 wt% to 75 wt%, then slightly decreased at 100 wt% and decreased more at 200 wt%. The highest spin density was calculated to be 1.35×10^{20} cm^{-3} based on a Bruker calibration sample. This is of the same order of magnitude as the repeat unit number density. The ultraviolet photoelectron spectroscopy (UPS) spectra are shown in **Figure 2d** and S5a. The secondary electron cutoff of PFClTVT doped by 50 wt% PSpF shifts by -0.23 eV, suggesting a downward movement of its Fermi level by 0.23 eV[34] which is similar to the TBAF doped polymer films.[25a] and could be from associations of the doped polymer with multiple cations of the dopant or a surface voltage induced by the dopant.

The electrical conductivity of doped polymer films was examined by a four-probe method and the Seebeck coefficients were determined by detecting the thermoelectric voltages under different temperature gradients ΔT. All the measurements were performed in the open air. All the doped films exhibit reasonably high σ over 1 S cm^{-1} except polymer films doped by 1 wt% PSpF, indicating PSpF doped polymer films can give effective electron transport over a broad range of dopant concentration (The F^-/PFClTVT ratio is between 4.7 and 188 mol%, Figure S5d), which is very different from N-DMBI doped films,[15, 28a, 36] suggesting a broad process window for polymer dopant PSpF; polymers with 100 wt% PSpF doping show the highest σ of 4.2 S cm^{-1} (**Figure 3a**). The Seebeck coefficients for 1, 5, 30, 50, 75, 100 and

200 wt% are 649±75, 476±7, -455±10, -432±31, -354±28, -316±11 and 550±100 μV K^{-1}, respectively (**Figure 3b**); the *S* are relatively consistent in the PSpF fraction range between 1-200 wt% compared to N-DMBI-based devices,[28a] suggesting high concentration-tolerance of PSpF doping. The highest power factor of 75 (67±8) μW m^{-1} K^{-2} was achieved for 200 wt% PSpF doped films with the contribution of relatively high σ relative to *S* (**Figure 3c**). PFClTVT doped by 200 wt% PSpF exhibits relatively high electrical conductivity and power factor of 2 S cm^{-1} and 67 μW m^{-1} K^{-2}, respectively. The lowest *PF* is 28 μW m^{-1} K^{-2} with 30 wt% PSpF doping; even that *PF* is still much higher than for most n-type organic thermoelectrics.[9]

Thermal conductivity measurements on the thin film samples were performed via time-domain thermoreflectance (TDTR) to study the effect of polystyrene-based dopant PSpF on that property.[37] The thermal conductivities of pristine PFClTVT and PSpF are about 0.25±0.07 and 0.11±0.04 W m^{-1} K^{-1} (**Figure 3d**), respectively. The thermal conductivity of PSpF-doped PFClTVT films decreased from 0.22±0.07 W m^{-1} K^{-1} to 0.16±0.04 W m^{-1} K^{-1} when the dopant concentration increased from 5 to 100 wt%, suggesting PSpF can decrease the thermal conductivity of doped polymer films in proportion to its compositional fraction. The sources of uncertainty in our reported values for thermal conductivity measurements on these thin films polymer samples are reported in our prior works.[20, 25a] The highest *ZT*, assuming isotropic orientation of drop-cast films, is calculated to be about 0.1.

To explore the relationship of *S*, *PF* and σ, the Seebeck coefficient and power factor as functions of electrical conductivity in this work were compared with reported works which have been summarized by Russ et al (Figure S6).[17] Though the *S* and *PF* (Figure S6) in this work are relatively high, they are still reasonable and very similar to the trend of p-type thermoelectrics based on PEDOT:PSS.[38]

The thermal stability in the ambient atmosphere is very important for thermoelectric devices. It was explored by recording the electrical conductivity of films with 75 wt% PSpF doping before and after thermal treatment at 120 ℃ for 2 cycles of 15 min in the open air. The σ at room temperature was 3.45 S cm^{-1} before thermal treatment; after 2 cycles of 15 min thermal treatment, the value of 3.39 S cm^{-1} was achieved, an insignificant 2% decrease (Figure S5c). The σ values decreased about 1-10% at 28-57 ℃, exhibiting excellent thermal stability in the open air. Moreover, the apparent E_a hardly changed in the process. The doped film also shows good ambient stability; the σ was 2.35±0.27 S cm^{-1} upon 9 days exposure to air, only a 24-40% decrease. Considering that the thickness of the films was only 100-300 nm, the ambient stability is outstanding. To compare the thermal stability with that from a conventional dopant, 100 wt% PSpF and 50 mol% N-DMBI doped PFClTVT films were measured under the same condition; the result is shown in **Figure 4a and 4b**. After 4 cycles of 15 min thermal treatment, the σ values of PSpF doped PFClTVT decreased about 4-14% at 32-85 ℃, the σ values at room temperature decresed from 4.2 S cm^{-1} to 3.9 S cm^{-1}, a low decrement of 7% was observed. While, the significant of 37-50% decrease was observed in N-DMBI doped PFClTVT films after 4 cycles of 15 min thermal treatment, which is much higher than PSpF doped PFClTVT. The σ value of N-DMBI doped PFClTVT at room temperature was 36.8 S cm^{-1}, and decreased to 21.8 S cm^{-1} after 4 cycles of 15 min thermal treatment; a high decrement of 41% was observed. The stability of PSpF doped PFClTVT is probably promoted by the fragments of PS in PSpF that could block the access of water and/or oxygen to the mobile electrons.

To estimate the activation energy (E_a) of doped polymer films, temperature-dependent electrical conductivity values of PFClTVT with 30 wt% PSpF doping were recorded in **Figure 4c**. The PSpF doped film shows increasing σ values over the range of 25-90 ℃. The

apparent E_a was calculated according to the Arrhenius equation, being 282 meV. The value of the activation energy divided by the average temperature of the measurement is 852 μV K^{-1}.[39] The value is somewhat higher than the measured Seebeck coefficient due to the barrier to site-to-site hopping, but is of the same order of magnitude as *S*. The time-dependent thermoelectric voltage responses under different temperature gradients were recorded for 36 minutes (**Figure 4d**). These were very stable, suggesting the relatively high Seebeck coefficient can most likely originate from an electron contribution, not from ion contributions.[40]

Electron mobility plays a key role in electrical conductivity, according to the formulation $\sigma = ne\mu$, where n is carrier density, e is electron charge and μ is the corresponding carrier mobility. The σ is positively related to μ and n of polymer films.[41] To measure the electrical mobility of doped polymer films, organic field effect transistors (OFETs) with top-gate/bottom-contact (TGBC) configuration were prepared and studied. The dopant PSpF fractions in the OFETs are 1, 2 and 10 wt%. The transfer and output curves are shown in **Figure 5**, Figure S8 and S9 in the supporting information. The performance of OFETs is summarized in Table S2. In the transfer curves, PFClTVT with 1 wt% PSpF doping shows much higher I_d than pristine films, while, in the output curves, 1 wt% PSpF doped films show better linear behavior than undoped films in the low V_d region, owing to the reduction of contact resistance.[25b] PFClTVT with 1 wt% PSpF doping shows a high electron mobility of 0.81 ± 0.05 cm^2 V^{-1} s^{-1}, much higher than the mobility of undoped PFClTVT of 0.24 ± 0.04 cm^2 V^{-1} s^{-1}. This could be from the filling of traps and/or the dopant inducing locally improved order. When the dopant fraction increases to 2 and 10 wt%, the electron mobility decreases to 0.37 ± 0.01 and 0.13 ± 0.05 cm^2 V^{-1} s^{-1}, respectively, presumably because the unconjugated polymer dopant can disorder the conjugated polymer arrangement. The results are also further supported by a Hall effect measurement. A high electron mobility of 1.70 cm^2 V^{-1} s^{-1} was

achieved in 50 wt% PSpF doped PFClTVT films, which is much higher than 0.97 $cm^2 V^{-1} s^{-1}$ in pristine PFClTVT films.

Polymer film microstructures were determined by grazing incidence X-ray scattering (GIXRS). The strong diffraction peaks of (100) and (200) were detected for pristine and 5-75 wt% PSpF doped polymer films, suggesting polymer molecules are in an ordered arrangement when the fraction of PFClTVT is higher than PSpF (Figure S7a). There is no (010) peak detected in the out-of-plane diffractions, indicating the polymer films have an edge-on orientation packing. With the fractions of PSpF increasing from 0 to 75 wt%, the lamellar *d*-spacing distance increases from 30.15 to 32.97 Å (Figure S7b), possibly indicating some intercalation of polystyrene segments within the nonpolar parts of the conjugated polymers. PFClTVT with 100 wt% PSpF doping presents a smaller *d*-spacing distance (32.17 Å) than that of 75 wt% PSpF doping and a much weaker (100) peak, suggesting further change and disorder of the polymer arrangements if this d-spacing difference is considered significant. The (200) peak width decreases linearly as the PSpF fraction increases from 0 to 100 wt% (Figure S9), suggesting PSpF likely can make alkyl side chains more compact.[42] The surface morphology of polymer films was investigated by atomic force microscope (AFM). All the films present similar small size fiber-like aggregates with no preferred direction, suggesting good miscibility of PSpF with conjugated polymers (Figure S11). The smaller root-mean-square roughness of polymer film with 100 wt% PSpF doping is attributed to the low crystallinity (implying little or no preferred orientation) consistent with the GIXRS result.

To further study the morphology and doping reaction of PFClTVT and PSpF, scanning electron microscope (SEM) and energy dispersive spectroscopy (EDS) measurements were done to examine the films prepared by drop-casting on Si/SiO_2 substrates. The micron-sized

aggregates can be observed in 5 and 50 wt% PSpF doped PFClTVT films (**Figure 6**), indicating the phase separation between the ionic polymer PSpF and conjugated polymer PFClTVT. There is no F detected in pure PSpF film because F^- can escape as HF in high vacuum. The content of F atoms increased from 0.14% in pristine PFClTVT to 0.96% in 5 wt% PSpF doped PFClTVT (Table s3, 4 and 5), due to the reaction of F^- with BDOPV rings in PFClTVT.[25a] The results indicate that the F atoms are covalently bonded to the polymer after doping.

We already proposed that the electron-rich F^- can react with the strong electron-withdrawing unit BDOPV to form a radical anion.[25a] In the doping process, F^- is the effective part and PSP^+ will act as the counterion to compensate for the negative charge on the $PFClTVTF^-$ polymer chain. In the present case, the electron-rich F^- can react with the similarly strong electron-withdrawing unit and form anionic Meisenheimer complexes $PFClTVTF^-$, from which mobile electrons are transferred to other polymer segments, as we have also previously discussed.[22] The doping reaction scheme is shown in **Figure 7**. The Meisenheimer complexes are stable because the F is covalently bonded to the polymer PFClTVT, as we confirmed by the EDS measurement. The PSP^+ cation remains as the counterion for the F- complexes. The $PFClTVTF^-$ radical anion can be the vehicle for transporting electrons, and PSP cations are relatively stationary and could be local electron traps. The polymer dopant is non-conducting because of the dominant polystyrene groups, and can enhance the Seebeck coefficients because of the trapping (locally decreased electron energy levels) and possible energy-filtering barriers.

The results demonstrate that the copolymer PSpF can be an effective n-dopant for high-performance n-type organic thermoelectrics. High electrical conductivity of 4.2 S cm^{-1} and power factor of 67 μW m^{-1} K^{-2} were achieved for PSpF doped polymer films. The OFETs of

PSpF doped thin films exhibit high electron mobility of 0.86 $cm^2 V^{-1} s^{-1}$. Moreover, excellent thermal stability and ambient stability were observed for the electrical conductivity of PSpF doped films. Very stable time-dependent thermoelectric voltage responses under different temperature gradients were recorded. This work opens the way for designing polymer n-type dopants for organic conductors and thermoelectrics with low thermal conductivity, high conductivity relative to-Seebeck coefficient and high power factor.

Supporting Information
Supporting Information is available from the Wiley Online Library or from the author.

Acknowledgements

This work was primarily supported by the National Science Foundation, Division of Chemistry, grant numbers 1708245 and 2107360. We thank Baixiang Li and Yuyang Ji for their help with GPC measurement. We acknowledge Lisa Pogue and Tyrel McQueen for assistance and training on the x-ray diffractometer. We also appreciate support from the Office of Naval Research, grant number N00014-20-1-2686.

Received: ((will be filled in by the editorial staff))
Revised: ((will be filled in by the editorial staff))
Published online: ((will be filled in by the editorial staff))

References:

[1] A. F. Paterson, A. Savva, S. Wustoni, L. Tsetseris, B. D. Paulsen, H. Faber, A. H. Emwas, X. Chen, G. Nikiforidis, T. C. Hidalgo, M. Moser, I. P. Maria, J. Rivnay, I. McCulloch, T. D. Anthopoulos, S. Inal, *Nat. Commun.* **2020**, *11*, 3004.

[2] Y. Han, H. Zhao, C. Duan, S. Yang, Z. Yang, Z. Liu, S. Liu, *Adv. Funct. Mater.* **2020**, *30*, 1909972.

[3] H. L. Smith, J. T. Dull, E. Longhi, S. Barlow, B. P. Rand, S. R. Marder, A. Kahn, *Adv. Funct. Mater.* **2020**, *30*, 2000328.

[4] J. Graciani, A. Nambu, J. Evans, J. A. Rodriguez, J. F. Sanz, *J. Am. Chem. Soc.* **2008**, *130*, 12056-12063.

[5] a) H. Chen, M. Moser, S. Wang, C. Jellett, K. Thorley, G. T. Harrison, X. Jiao, M. Xiao, B. Purushothaman, M. Alsufyani, H. Bristow, S. De Wolf, N. Gasparini, A. Wadsworth, C. R. McNeill, H. Sirringhaus, S. Fabiano, I. McCulloch, *J. Am. Chem. Soc.* **2021**, *143*, 260-268; b) Y. Lu, J.-Y. Wang, J. Pei, *Acc. Chem. Res.* **2021**, *54*, 2871-2883; c) M. Xiong, X. Yan, J.-T. Li, S. Zhang, Z. Cao, N. Prine, Y. Lu, J.-Y. Wang, X. Gu, T. Lei, *Angew. Chem. Int. Ed.* **2021**, *60*, 8189-8197; d) A. Tripathi, Y. Lee, S. Lee, H. Y. Woo, *Journal of Materials Chemistry C* **2022**.

[6] a) S. Yang, P. Qiu, L. Chen, X. Shi, *Small Science* **2021**, *1*, 2100005; b) Y. Zhang, S.-J. Park, *Polymers* **2019**, *11*, 909; c) Y. Zhao, L. Liu, F. Zhang, C.-a. Di, D. Zhu, *SmartMat* **2021**, *DOI:10.1002/smm2.1034*.

[7] Y. Xia, K. Sun, J. Ouyang, *Adv. Mater.* **2012**, *24*, 2436-2440.

[8] J. G. Tait, B. J. Worfolk, S. A. Maloney, T. C. Hauger, A. L. Elias, J. M. Buriak, K. D. Harris, *Sol. Energy Mater. Sol. Cells* **2013**, *110*, 98-106.

[9] Y. Lu, J.-Y. Wang, J. Pei, *Chem. Mater.* **2019**, *31*, 6412-6423.

[10] Y. Sun, C.-A. Di, W. Xu, D. Zhu, *Adv. Electron. Mater.* **2019**, *5*, 1800825.

[11] H. Guo, C.-Y. Yang, X. Zhang, A. Motta, K. Feng, Y. Xia, Y. Shi, Z. Wu, K. Yang, J. Chen, Q. Liao, Y. Tang, H. Sun, H. Y. Woo, S. Fabiano, A. Facchetti, X. Guo, *Nature* **2021**, *599*, 67-73.

[12] X. Yan, M. Xiong, X.-Y. Deng, K.-K. Liu, J.-T. Li, X.-Q. Wang, S. Zhang, N. Prine, Z. Zhang, W. Huang, Y. Wang, J.-Y. Wang, X. Gu, S. K. So, J. Zhu, T. Lei, *Nat. Commun.* **2021**, *12*, 5723.

[13] C. Dong, S. Deng, B. Meng, J. Liu, L. Wang, *Angew. Chem. Int. Ed.* **2021**, *60*, 16184-16190.

[14] Y. Wang, K. Takimiya, *Adv. Mater.* **2020**, *32*, 2002060.

[15] W. Ma, K. Shi, Y. Wu, Z. Y. Lu, H. Y. Liu, J. Y. Wang, J. Pei, *ACS Appl. Mater. Inter.* **2016**, *8*, 24737-24743.

[16] C. Y. Yang, W. L. Jin, J. Wang, Y. F. Ding, S. Nong, K. Shi, Y. Lu, Y. Z. Dai, F. D. Zhuang, T. Lei, C. A. Di, D. Zhu, J. Y. Wang, J. Pei, *Adv. Mater.* **2018**, *30*, e1802850.

[17] B. Russ, A. Glaudell, J. J. Urban, M. L. Chabinyc, R. A. Segalman, *Nat. Rev. Mater.* **2016**, *1*, 16050.

[18] a) Q. Zhang, Y. Sun, W. Xu, D. Zhu, *Adv. Mater.* **2014**, *26*, 6829-6851; b) Y. Chen, Y. Zhao, Z. Liang, *Energy Environ. Sci.* **2015**, *8*, 401-422.

[19] a) W. Park, J. Hu, L. A. Jauregui, X. Ruan, Y. P. Chen, *Applied Physics Letters* **2014**, *104*, 113101; b) M. B. Jakubinek, M. A. White, M. Mu, K. I. Winey, *Applied Physics Letters* **2010**, *96*, 083105; c) S. A. Al-Ajlan, *Appl. Therm. Eng.* **2006**, *26*, 2184-2191.

[20] H. Li, M. E. DeCoster, R. M. Ireland, J. Song, P. E. Hopkins, H. E. Katz, *Journal of the American Chemical Society* **2017**, *139*, 11149-11157.

[21] K. F. Seidel, D. Lungwitz, A. Opitz, T. Krüger, J. Behrends, S. R. Marder, N. Koch, *ACS Appl. Mater. Interfaces* **2020**, *12*, 28801-28807.

[22] C.-Y. Yang, M.-A. Stoeckel, T.-P. Ruoko, H.-Y. Wu, X. Liu, N. B. Kolhe, Z. Wu, Y. Puttisong, C. Musumeci, M. Massetti, H. Sun, K. Xu, D. Tu, W. M. Chen, H. Y. Woo, M. Fahlman, S. A. Jenekhe, M. Berggren, S. Fabiano, *Nat. Commun.* **2021**, *12*, 2354.

[23] K. Xu, H. Sun, T.-P. Ruoko, G. Wang, R. Kroon, N. B. Kolhe, Y. Puttisong, X. Liu, D. Fazzi, K. Shibata, C.-Y. Yang, N. Sun, G. Persson, A. B. Yankovich, E. Olsson, H. Yoshida, W. M. Chen, M. Fahlman, M. Kemerink, S. A. Jenekhe, C. Müller, M. Berggren, S. Fabiano, *Nat. Mater.* **2020**, *19*, 738-744.

[24] K. Naoi, M. Lien, W. H. Smyrl, *J. Electrochem. Soc.* **1991**, *138*, 440-445.

[25] a) X. Zhao, D. Madan, Y. Cheng, J. Zhou, H. Li, S. M. Thon, A. E. Bragg, M. E. DeCoster, P. E. Hopkins, H. E. Katz, *Adv. Mater.* **2017**, *29*, 1606921; b) J. Kim, D. Khim, K.-J. Baeg, W.-T. Park, S.-H. Lee, M. Kang, Y.-Y. Noh, D.-Y. Kim, *Adv. Funct.*

Mater. **2016**, *26*, 7886-7894.

[26] J. Han, C. Ganley, Q. Hu, X. Zhao, P. Clancy, T. P. Russell, H. E. Katz, *Adv. Funct. Mater.* **2021**, *31*, 2010567.

[27] K. Cui, X. Lu, W. Cui, J. Wu, X. Chen, Q. Lu, *Commun. Chem.* **2011**, *47*, 920-922.

[28] a) J. Han, H. Fan, Q. Zhang, Q. Hu, T. P. Russell, H. E. Katz, *Adv. Funct. Mater.* **2021**, *31*, 2005901; b) A. Marks, X. Chen, R. Wu, R. B. Rashid, W. Jin, B. D. Paulsen, M. Moser, X. Ji, S. Griggs, D. Meli, X. Wu, H. Bristow, J. Strzalka, N. Gasparini, G. Costantini, S. Fabiano, J. Rivnay, I. McCulloch, *Journal of the American Chemical Society* **2022**, *144*, 4642-4656; c) M. Alsufyani, M.-A. Stoeckel, X. Chen, K. Thorley, R. K. Hallani, Y. Puttisong, X. Ji, D. Meli, B. D. Paulsen, J. Strzalka, K. Regeta, C. Combe, H. Chen, J. Tian, J. Rivnay, S. Fabiano, I. McCulloch, *Angew. Chem. Int. Ed.* **2022**, *61*, e202113078.

[29] G. Moad, E. Rizzardo, S. H. Thang, *Chem-Asian J.* **2013**, *8*, 1634-1644.

[30] T. Li, C. Zhou, M. Jiang, *Polym. Bull.* **1991**, *25*, 211-216.

[31] a) C. S. Abeywickrama, Y. Pang, *New J. Chem.* **2021**, *45*, 9102-9108; b) X. Liu, X. Liu, Y. Shen, B. Gu, *ACS Omega* **2020**, *5*, 21684-21688.

[32] B. D. Naab, X. Gu, T. Kurosawa, J. W. F. To, A. Salleo, Z. Bao, *Adv. Electron. Mater.* **2016**, *2*, 1600004.

[33] J. L. Bredas, G. B. Street, *Acc. Chem. Res.* **1985**, *18*, 309-315.

[34] X. Yan, M. Xiong, J. T. Li, S. Zhang, Z. Ahmad, Y. Lu, Z. Y. Wang, Z. F. Yao, J. Y. Wang, X. Gu, T. Lei, *J. Am. Chem. Soc.* **2019**, *141*, 20215-20221.

[35] M. Massetti, F. Jiao, A. J. Ferguson, D. Zhao, K. Wijeratne, A. Würger, J. L. Blackburn, X. Crispin, S. Fabiano, *Chem. Rev.* **2021**, *121*, 12465-12547.

[36] a) K. Shi, F. Zhang, C. A. Di, T. W. Yan, Y. Zou, X. Zhou, D. Zhu, J. Y. Wang, J. Pei, *J. Am. Chem. Soc.* **2015**, *137*, 6979-6982; b) J. Liu, B. van der Zee, R. Alessandri, S. Sami, J. Dong, M. I. Nugraha, A. J. Barker, S. Rousseva, L. Qiu, X. Qiu, N. Klasen, R.

C. Chiechi, D. Baran, M. Caironi, T. D. Anthopoulos, G. Portale, R. W. A. Havenith, S. J. Marrink, J. C. Hummelen, L. J. A. Koster, *Nature Communications* **2020**, *11*, 5694; c) C.-Y. Yang, Y.-F. Ding, D. Huang, J. Wang, Z.-F. Yao, C.-X. Huang, Y. Lu, H.-I. Un, F.-D. Zhuang, J.-H. Dou, C.-a. Di, D. Zhu, J.-Y. Wang, T. Lei, J. Pei, *Nature Communications* **2020**, *11*, 3292; d) J. Han, A. Chiu, C. Ganley, P. McGuiggan, S. M. Thon, P. Clancy, H. E. Katz, *Angew. Chem. Int. Ed.* **2021**, *60*, 27212-27219; e) Y. Lu, Z.-D. Yu, H.-I. Un, Z.-F. Yao, H.-Y. You, W. Jin, L. Li, Z.-Y. Wang, B.-W. Dong, S. Barlow, E. Longhi, C.-a. Di, D. Zhu, J.-Y. Wang, C. Silva, S. R. Marder, J. Pei, *Adv. Mater.* **2021**, *33*, 2005946.

[37] a) D. G. Cahill, *Review of Scientific Instruments* **2004**, *75*, 5119-5122; b) J. L. Braun, S. W. King, A. Giri, J. T. Gaskins, M. Sato, T. Fujiseki, H. Fujiwara, P. E. Hopkins, *Applied Physics Letters* **2016**, *109*, 191905.

[38] G. H. Kim, L. Shao, K. Zhang, K. P. Pipe, *Nat. Mater.* **2013**, *12*, 719-723.

[39] a) N. F. Mott, E. A. Davis, *Electronic processes in non-crystalline materials*, Oxford university press, **2012**; b) D. Mendels, N. Tessler, *J. Appl. Phys.* **2015**, *117*, 105502.

[40] a) Y. Lu, Z.-D. Yu, Y. Liu, Y.-F. Ding, C.-Y. Yang, Z.-F. Yao, Z.-Y. Wang, H.-Y. You, X.-F. Cheng, B. Tang, J.-Y. Wang, J. Pei, *J. Am. Chem. Soc.* **2020**, *142*, 15340-15348; b) W. B. Chang, H. Fang, J. Liu, C. M. Evans, B. Russ, B. C. Popere, S. N. Patel, M. L. Chabinyc, R. A. Segalman, *ACS Macro Lett.* **2016**, *5*, 455-459.

[41] K. S. Novoselov, A. K. Geim, S. V. Morozov, D. Jiang, Y. Zhang, S. V. Dubonos, I. V. Grigorieva, A. A. Firsov, *Science* **2004**, *306*, 666.

[42] K. Kang, S. Watanabe, K. Broch, A. Sepe, A. Brown, I. Nasrallah, M. Nikolka, Z. Fei, M. Heeney, D. Matsumoto, K. Marumoto, H. Tanaka, S.-i. Kuroda, H. Sirringhaus, *Nat. Mater.* **2016**, *15*, 896-902.

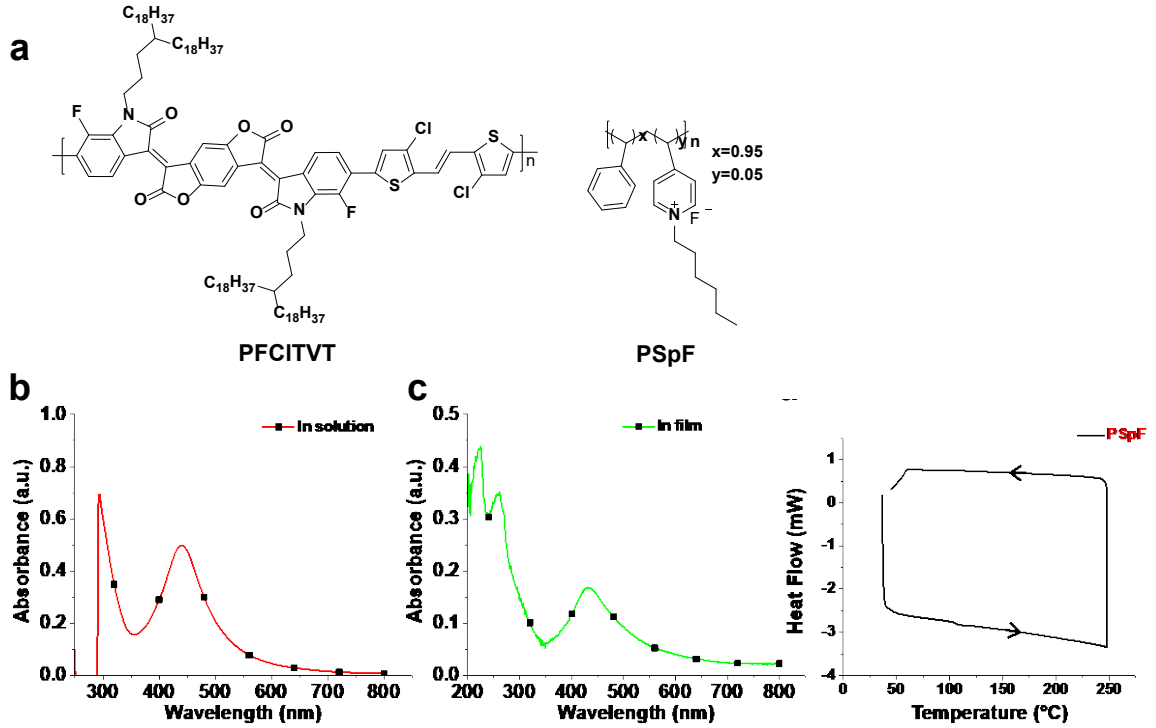

Figure 1. (a) Chemical structures of n-type conjugated polymer PFClTVT and dopant polymer PSpF. UV-vis-NIR absorption spectra of polymer dopant PSpF (b) in solution and (c) in film. (d) Differential scanning calorimeter (DSC) traces of PSpF measured under N_2.

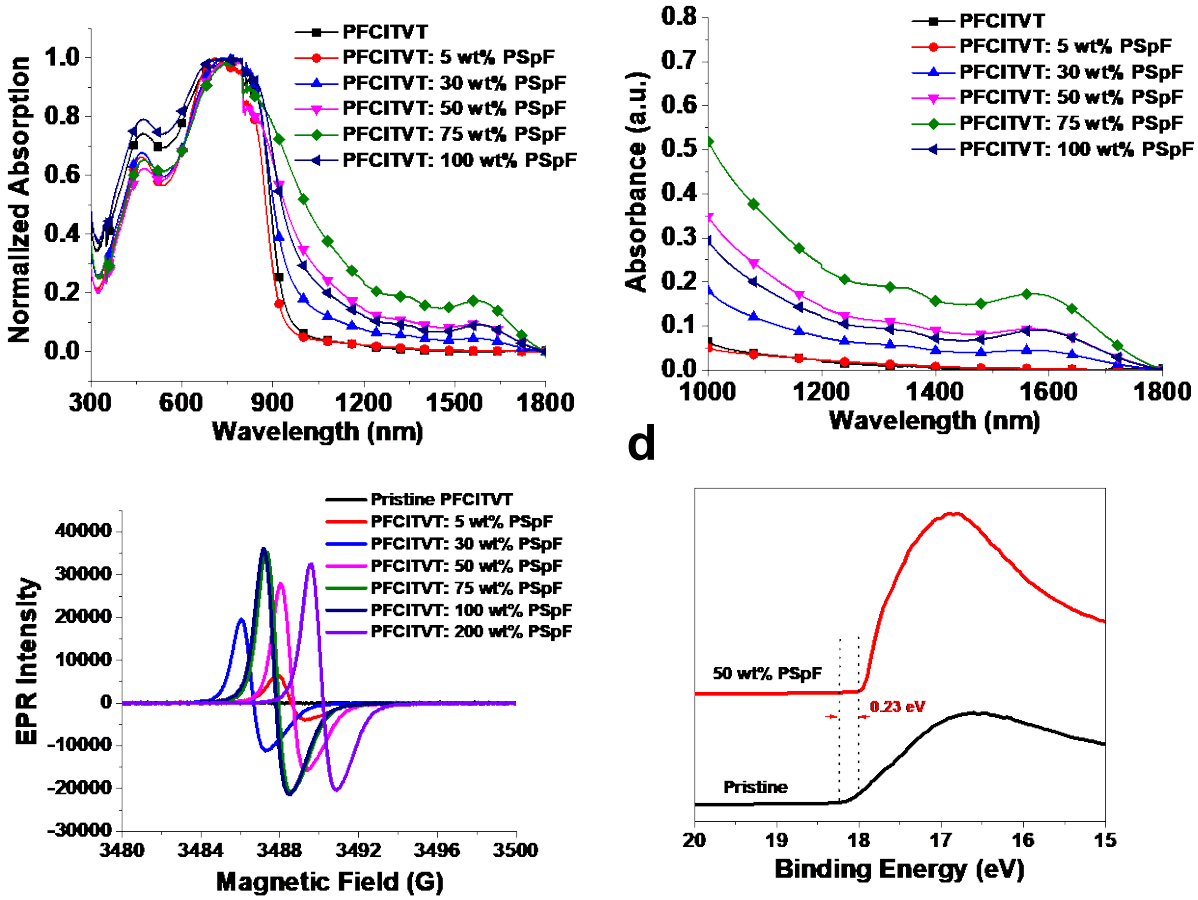

Figure 2. Normalized UV-vis-NIR absorption spectra of pristine PFClTVT and polymer films doped with different weight fractions of dopant (a) in UV-vis-NIR region and (b) in NIR region. (c) EPR spectra of pristine and doped polymer in solution. (d) UPS binding energy of the pristine and doped polymer films measured under -5 eV. The wt % in this paper means weight ratio of PSpF compared to the conjugated polymer PFClTVT, for example, 100 wt % means equal weights of conjugated polymer and PSpF.

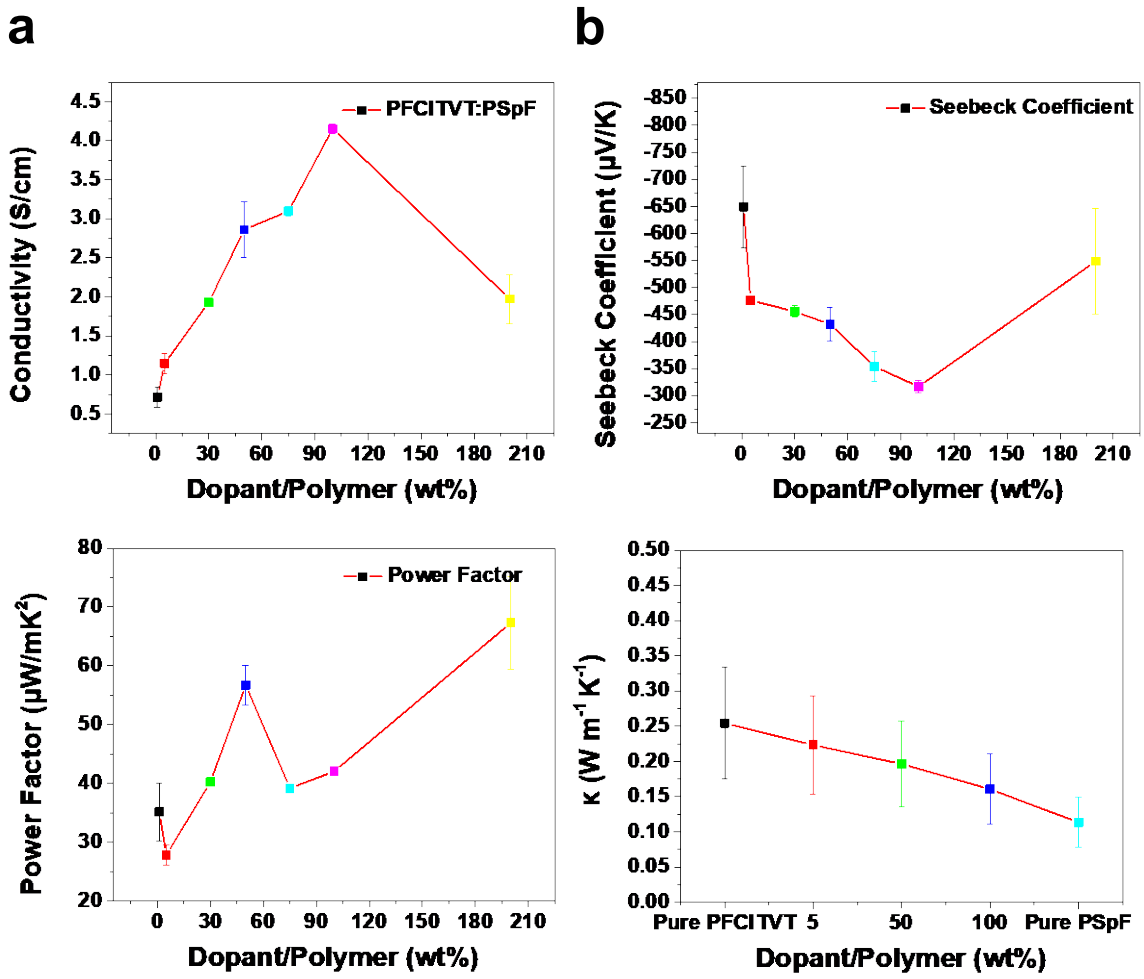

Figure 3. (a) Electrical conductivity, (b) Seebeck coefficient, (c) power factor and (d) thermal conductivity of PFClTVT films doped by various weight fractions of PSpF. The black spot in Figure 3a is 1 wt% PSpF doped, not undoped. Resistance was measured by using a four-probe method with a channel length of 1000 μm and a channel width of 140 μm. Seebeck coefficient were measured with a channel length of 2000 μm and a channel width of 8000 μm.

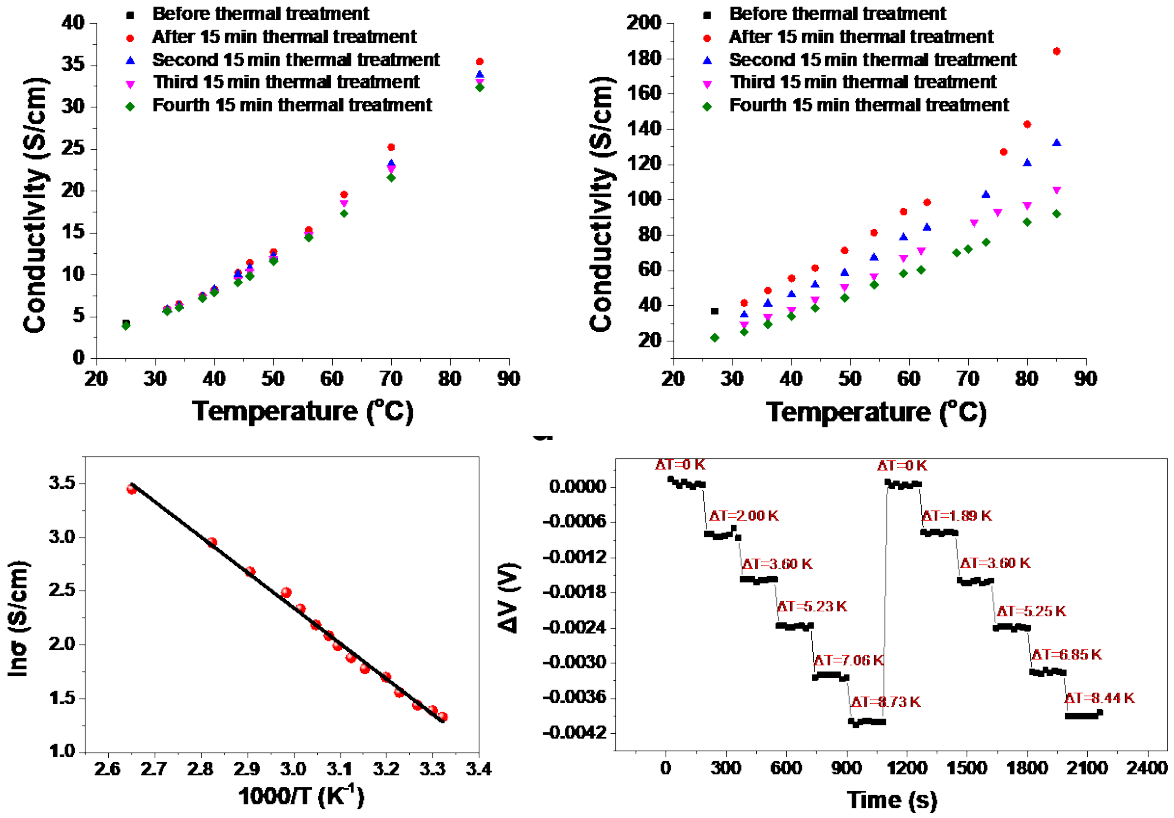

Figure 4. Thermal air stability of electrical conductivity of (a) PSpF and (b) N-DMBI doped PFClTVT films after thermal treatment at 120 ℃ for 4 cycles of 15 min in the open air. (c) Temperature-dependent electrical conductivity values of PFClTVT film doped with 30 wt% PSpF. (d) Time-dependent thermoelectric voltage response under different temperature gradients ΔT.

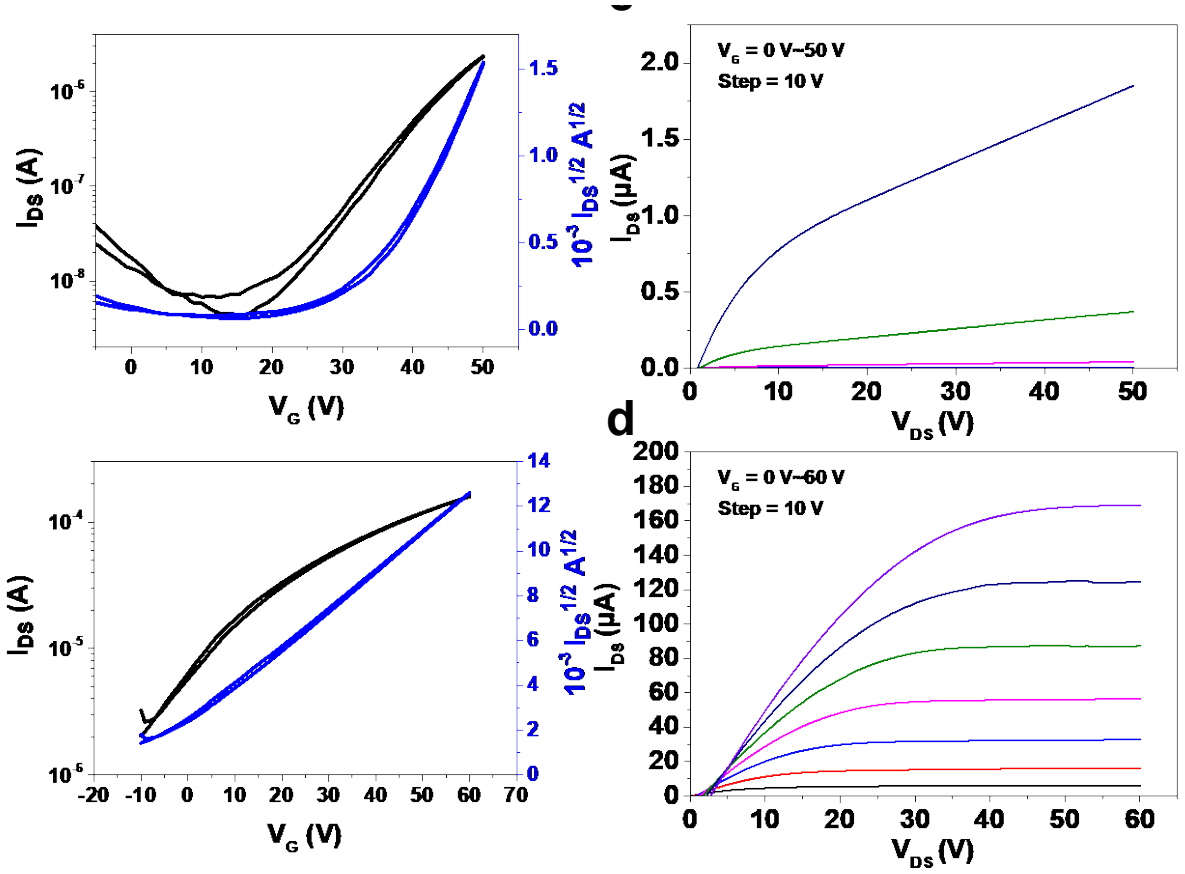

Figure 5. Transfer curves of (a) pristine and (b) 1 wt% PSpF doped OFETs. Output curves of (c) pristine and (d) 1 wt% PSpF doped OFETs. The OFETs were prepared with a channel length of 200 μm and a channel width of 8000 μm.

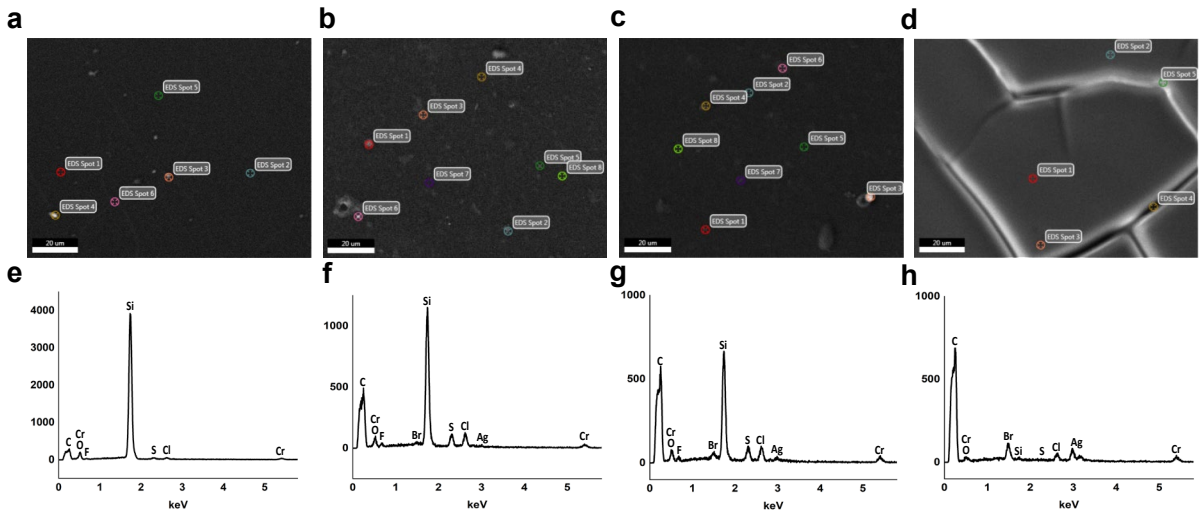

Figure 6. To measure SEM, polymer films were prepared by drop-casting which is in the same way with the all-polymer thermoelectrics. SEM images of (a) pristine PFClTVT, (b) 5 wt% PSpF, (c) 50 wt% PSpF doped PFClTVT and (d) pristine PSpF films. EDS analysis at the even area of (e) pristine PFClTVT (spot 1), (f) 5 wt% PSpF (spot 4), (g) 50 wt% PSpF doped PFClTVT (spot 5) and (h) pristine PSpF films (spot 1). The percentage composition of F in b and c is higher than a, suggesting the existence and adduct reaction with PFClTVT of F^- in PSpF.

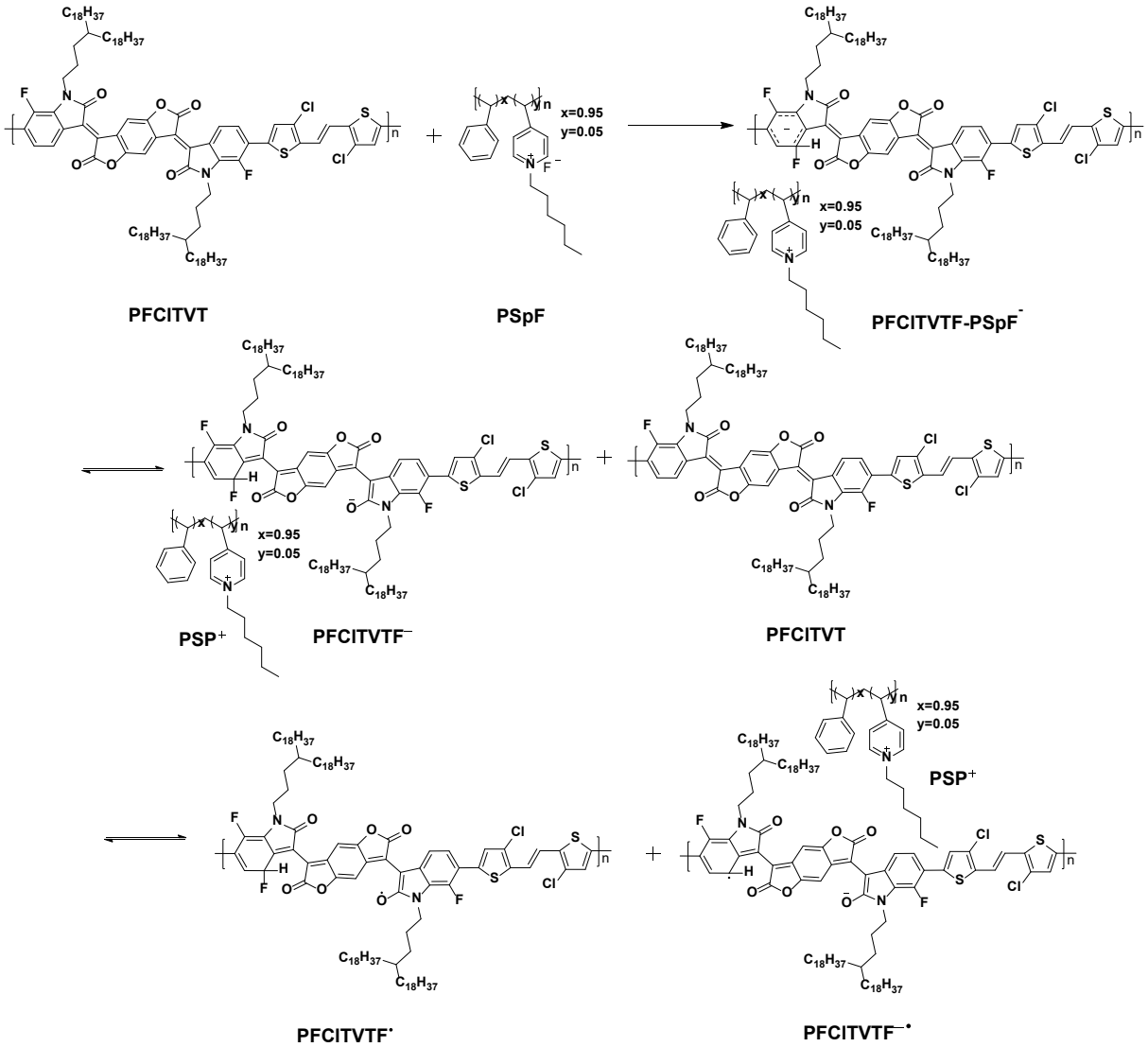

Figure 7. The proposed doping mechanism of polymer dopant PSpF and semiconducting polymer of PFClTVT. Other F^- addition sites and radical/anion resonance structures are possible.

A novel polystyrene-polyvinyl pyridinium-based n-type polymer dopant is firstly designed and synthesized. It can dope n-type conjugated polymers to make n-type all-polymer conducting materials and thermoelectrics, analogous to poly(3,4-ethylenedioxythiophene) poly(4-styrenesulfonate). High electrical conductivity of 4.2 S cm^{-1}, electron mobility of 0.86 $cm^2 V^{-1} s^{-1}$ and power factor of 67 μW $m^{-1} K^{-2}$ are achieved for PSpF doped polymer films.

Jinfeng Han, Emma Tiernan, Taein Lee, Arlene Chiu, Patty McGuiggan, Nicholas Adams, Patrick E. Hopkins, Susanna M. Thon, John D. Tovar, Howard E. Katz*

A New Polystyrene-Polyvinyl Pyridinium Ionic Copolymer Dopant for N-Type All-Polymer Thermoelectrics with High Stable Conductivity Relative to Seebeck Coefficient Giving High Power Factor

ToC figure

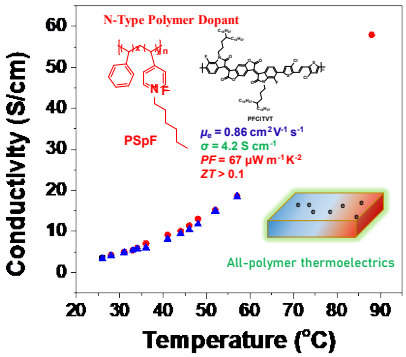

A New Polystyrene-Polyvinyl Pyridinium Ionic Copolymer Dopant for N-Type All-Polymer Thermoelectrics with High Stable Conductivity Relative to-Seebeck Coefficient Giving High Power Factor

Jinfeng Han[1], Emma Tiernan[2], Taein Lee[1], Arlene Chiu[3], Patty McGuiggan[1], Nicholas Adams[1], Patrick E. Hopkins[2], Susanna M. Thon[3], John D. Tovar[1], Howard E. Katz[1,]*

[1]Department of Materials Science and Engineering and Department of Chemistry, Johns Hopkins University, 3400 North Charles Street, Baltimore, Maryland 21218, United States

[2]Department of Mechanical and Aerospace Engineering, Department of Materials Science and Engineering (Courtesy) and Department of Physics (Courtesy), University of Virginia, 122 Engineer's Way, Charlottesville, VA 22904-4746, United States

[3]Department of Electrical and Computer Engineering, Johns Hopkins University, 3400 North Charles Street, Baltimore, Maryland 21218, United States

1. General procedures and experimental details.

Chemical reagents (Including solvent and PMMA) were purchased and used as received. All the synthesis procedures were performed under N_2.

^1H and ^{13}C NMR spectra were recorded on Bruker Advance (400 MHz) spectrometers. ^1H NMR chemical shifts were referenced to tetramethylsilane TMS (0 ppm). Gel permeation

chromatography (GPC) was performed on a PL gel MIXED-B LS 300 x 7.5mm x 3 at 150 ºC using trichlorobenzene (TCB) stabilized with 0.0125% BHT as eluent. The EPR measurements were performed on a Bruker-EMX EPR spectrometer at room temperature. Solutions of doped polymers were prepared by stirring at 120 ℃ for 3 min and then 50 μL solution was injected into EPR tubes. AFM images were taken in tapping mode using a Dimensional 3100 AFM (Bruker Nano, Santa Barbara, CA). The images were visualized using the Nanoscope software (Bruker). The absorption spectra were acquired on an Agilent Cary 5000 UV-Vis-NIR spectrophotometer. GIXRD was performed on a Bruker D8 Advance A25 instrument.

OFET Film Fabrication and Characterization.

Organic field electric transistors (OFETs) with top-gate/bottom-contact (TGBC) configuration were fabricated using n^{++}-Si/SiO2 (300 nm) substrates with a channel length of 200 μm and a channel width of 8000 μm. The substrates were cleaned using ultrasonication in cleaning agent (Decon, labs, Inc), deionized water, acetone, and isopropanol. The cleaned substrates were dried under vacuum at 60 ºC for 6 h and then transferred into a glovebox. The source and drain electrodes comprising a layer of Au (50 nm) were deposited through a shadow mask onto the silicon substrates by thermal evaporation. Thin films of polymers (2.5 mg/mL in orthodichlorobenzene (*o*-DCB)) and doped polymers were prepared by spin coating the solution on the substrates at 2000 rpm for 60 s and annealed at 150 ºC for 30 min. Then, the solution of PMMA was spin-coated on the polymer films at 2000 rpm for 60 s and annealed at 110 ºC for 30 min, resulting in a dielectric layer about 1050 nm thick. Gate electrodes comprising a layer of Au (50 nm) were then deposited through a shadow mask onto the dielectric layer by thermal evaporation. The OFET devices had a channel length (L) of 200

μm and a channel width (W) of 8000 μm. The evaluations of the OFETs were carried out in the ambient atmosphere on a probe stage using an Agilent B1500A as parameter analyzer. The mobility was calculated in the saturation regime according to the equation: $I_{DS} = (W/2L)\mu C_i(V_G - V_T)^2$, where I_{DS} is the drain current, μ is the mobility, and V_G and V_T are the gate voltage and threshold voltage, respectively.

Thermoelectric devices and properties measurements.

ITO electrodes with a channel length of 3 mm and a channel width of 7 mm patterned glass substrates were cleaned by sonication in cleaning agent, deionized water, acetone, and isopropanol. Polymer PFClTVT and PSpF were dissolved in *o*-DCB separately with the concentration of 2.5 and 10 mg mL^{-1}, respectively. N-DMBI was were dissolved in *o*-DCB with the concentration of 2.5 mg mL^{-1}. The polymers and the dopant solutions were heated at 100 ºC for 24 h. Then the polymer was blended with dopant in the desired weight ratio. The mixed solution was heated at 120 ºC and stirred for 2 min. The final solution was dropped on the glass substrates on which 2D wells are fabricated by laying a pattern of Novec polymer. After natural evaporation of solvent in a glove box over 24 h, square films form. The devices were annealed on a hot plate at 120 ºC for 12 h in nitrogen. All the measurements were performed in ambient. Resistance was measured by using a four-probe method with an Agilent B1500A Semiconductor Parameter Analyzer with a channel length of 1000 μm and a channel width of 140 μm. 3-8 measurements of resistance were performed on each sample surface in different positions. Seebeck coefficient can be calculated by $S=\Delta V/\Delta T$ with a channel length of 2000 μm and a channel width of 8000 μm, where ΔV is the thermal voltage obtained between the two electrodes of the device subjected to a temperature gradient ΔT. 2-4 Devices were measured for Seebeck coefficient measurement. Six ΔT were imposed on the sample, so the slopes of ΔV versus ΔT give values of the Seebeck coefficient.

Statistics

1. All the data in this work were processed by the software of OriginLab and without any normalization, except for the absorption spectra.
2. Data presentation: the data error bars were calculated and are shown as standard errors.
3. All the data were measured in different positions and repeated at different times with different devices. As noted above, for conductivity, at least 2 samples and 3-8 measurements at different positions on every sample; for Seebeck coefficient, at least 2 samples and 2-5 measurements at different positions on every sample.

2. Synthesis of polymers.

PFClTVT was synthesized according to the previous work.[1]

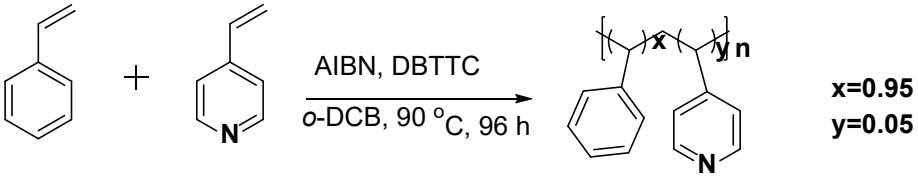

PS-P

PS-P: Styrene (20 g, 22.08 mL, 192 mmol) and vinylpyridine (1 g, 1.04 mL, 9.6 mmol) was added to a dry Schlenk tube under N_2, then 2, 2-azobisisobutyronitrile (AIBN) (12 mg) and S, S-Dibenzyl trithiocarbonate (DBTTC) (6 mg) was added to the Schlenk tube under N_2. Then 16 mL *o*-DCB was added to the tube, and evacuation and refilling with N_2 was repeated 8 times under stirring. Then the solution was heated to 90℃ and stirred for 96 h. The polymer solution was dropped into 350 mL methanol and stirred for 1 h, then it was filtered and washed in a Soxhlet extractor with methanol for 2 days. White solid was obtained in the yield of 85%. GPC: M_n = 118.4 kDa, M_w = 334.1 kDa, *PDI* = 2.8.

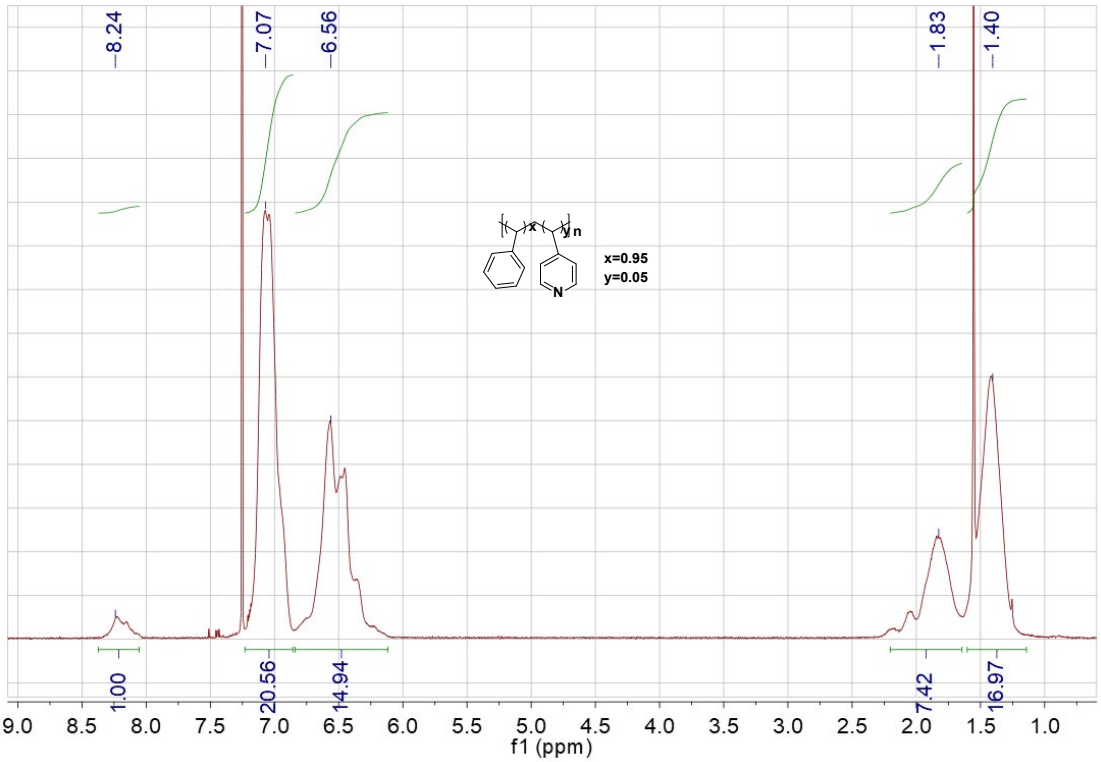

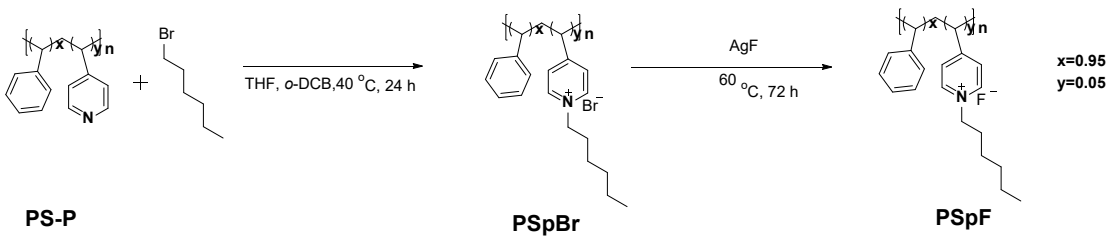

PS-P **PSpBr** **PSpF**

PSpBr: The polymer PS-P (3 g) and bromohexane (0.5 g) was added to a dry Schlenk bottle. Then 30 mL o-DCB and 10 mL THF was added and stirred for 0.5 h under N_2. Then the mixture was heated to 40℃ and reacted for 24 h. After reaction, the solution was cooled to room temperature and used in the next step without purification.

PSpF: Excess AgF (0.55 g) was added to the solution under N_2, and the mixture was heated to 60℃ and stirred for 72 h. After reaction, the solvent was removed with reduced pressure distillation. Then the solid was dissolved in chloroform and filtered. The filtrate was concentrated with rotary evaporation and dried in vacuum under 55 ℃ for 3 days. The faint yellow solid was obtained in the yield of 59%.

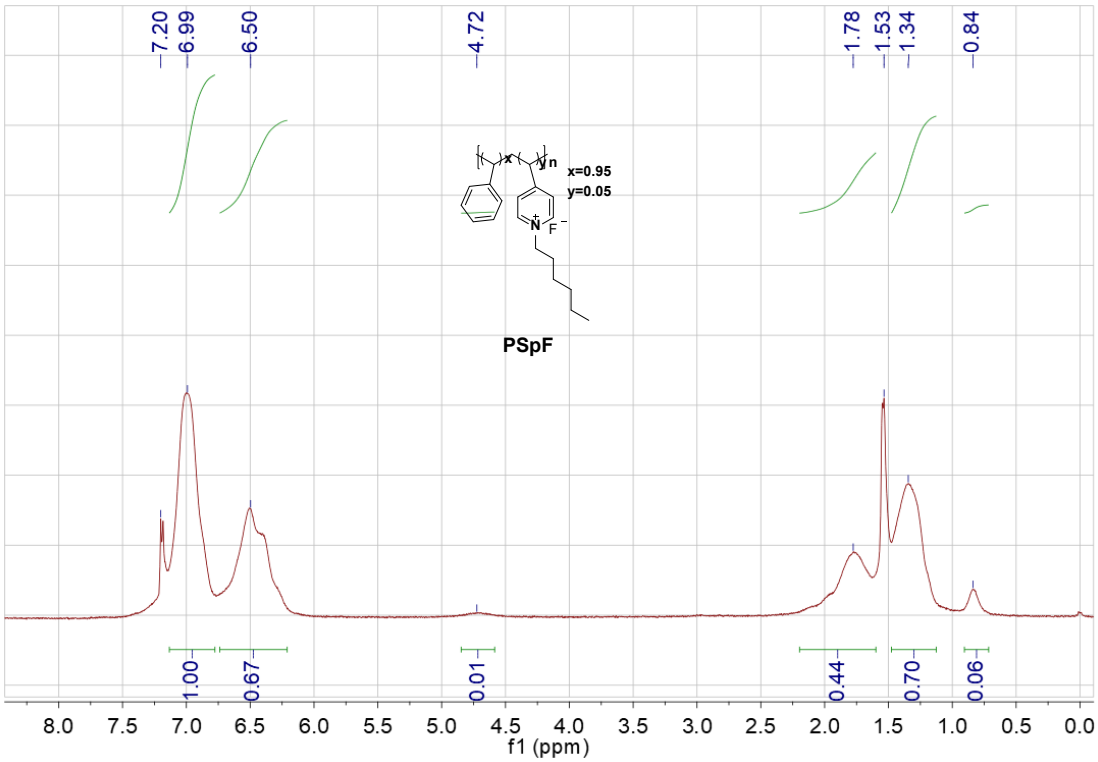

3. Characteristics of polymers and doped polymer films.

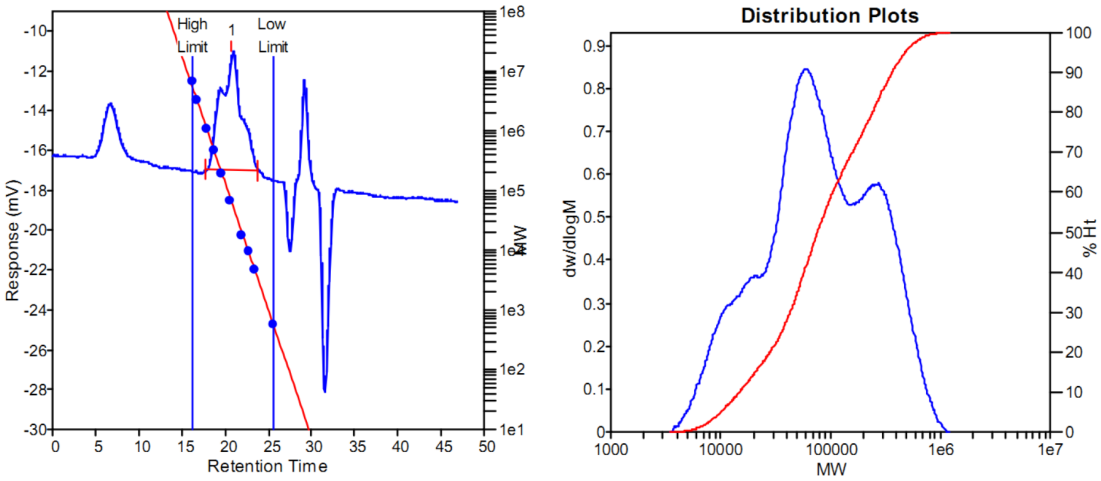

Figure 1. GPC spectra of PFClTVT.

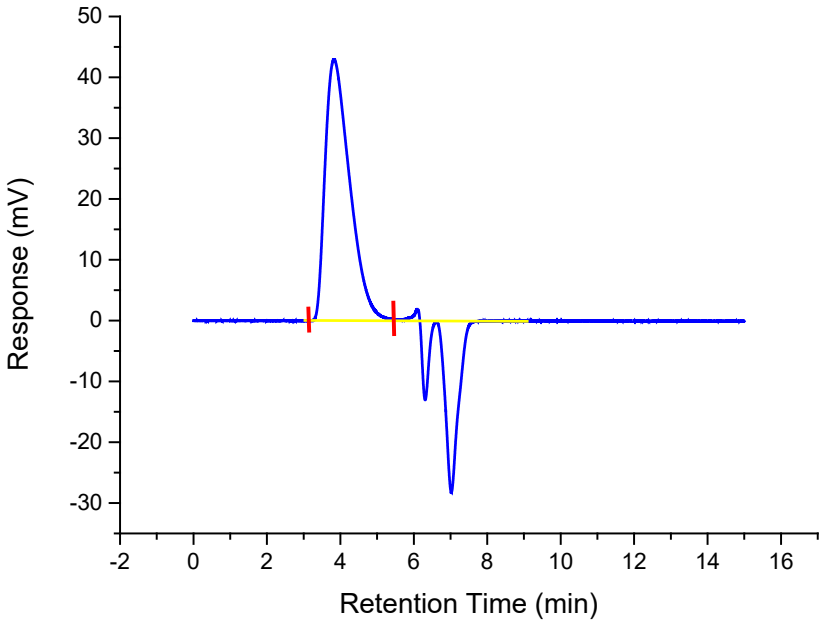

Figure 2. GPC spectra of PS-P.

Table 1. Characteristics of polymers. The molecular weight of PFClTVT was determined by GPC at 150 ℃ in 1,2,4-trichlorobenzene with polystyrene standards. The molecular weight of PS-P was determined by GPC at 30 ℃ in THF with polystyrene standards.

Polymer	M_n **(kDa)**	M_w **(kDa)**	***PDI***
PFClTVT	39.4	140.6	3.6
PS-P	118.4	334.1	2.8

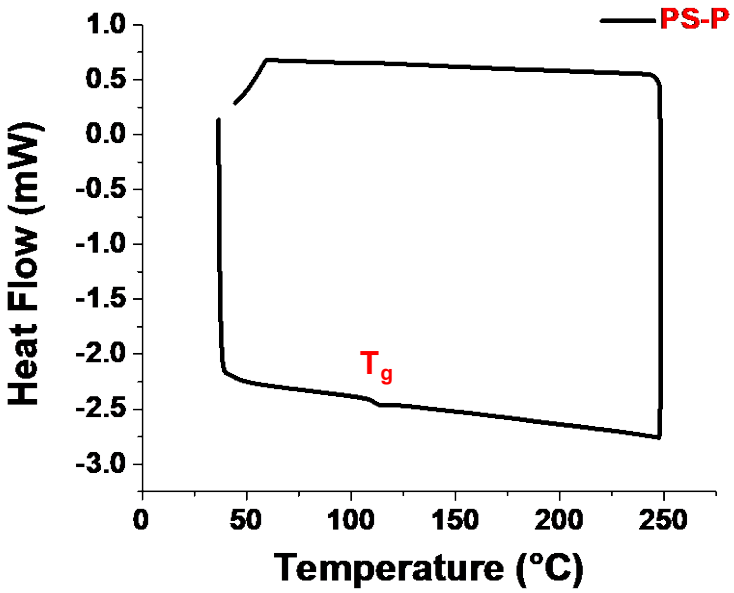

Figure 3. Differential scanning calorimeter (DSC) traces of PS-P measured under N_2.

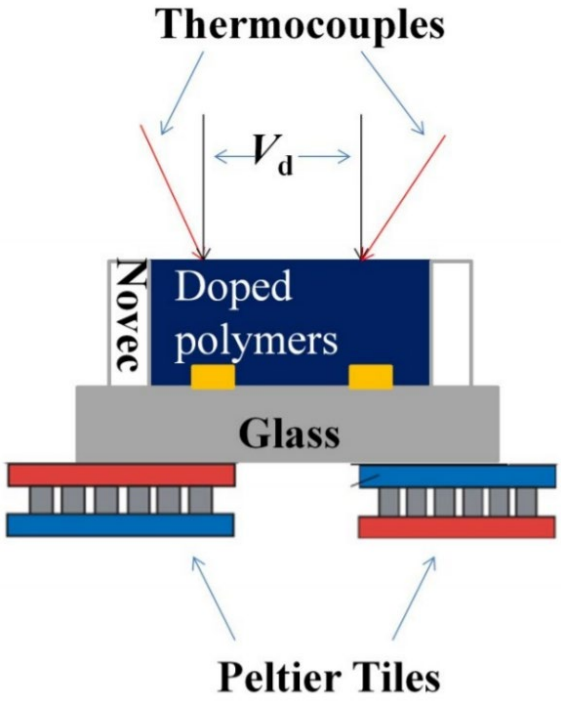

Figure 4. The sketch of the device cross-section used to estimate the Seebeck coefficient.[2]

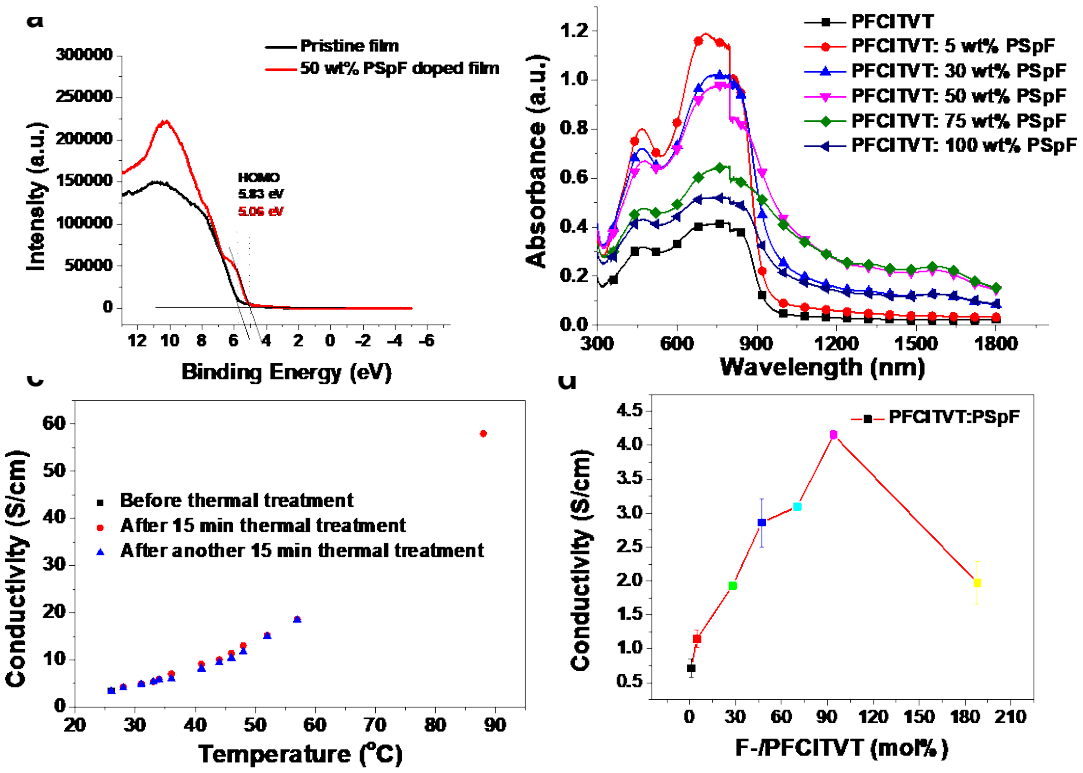

Figure 5. (a) UPS binding energy of the pristine and doped polymer films measured under -5 eV. (b) The normalized absorption of pristine and PSpF doped PFClTVT films. (c) Thermal air stability of electrical conductivity of 75 wt% PSpF doped PFClTVT films after thermal treatment at 120 °C for 2-circle 15 min in the open air. (d) The equivalent Figure 3a using F^- /PFClTVT mole ratio.

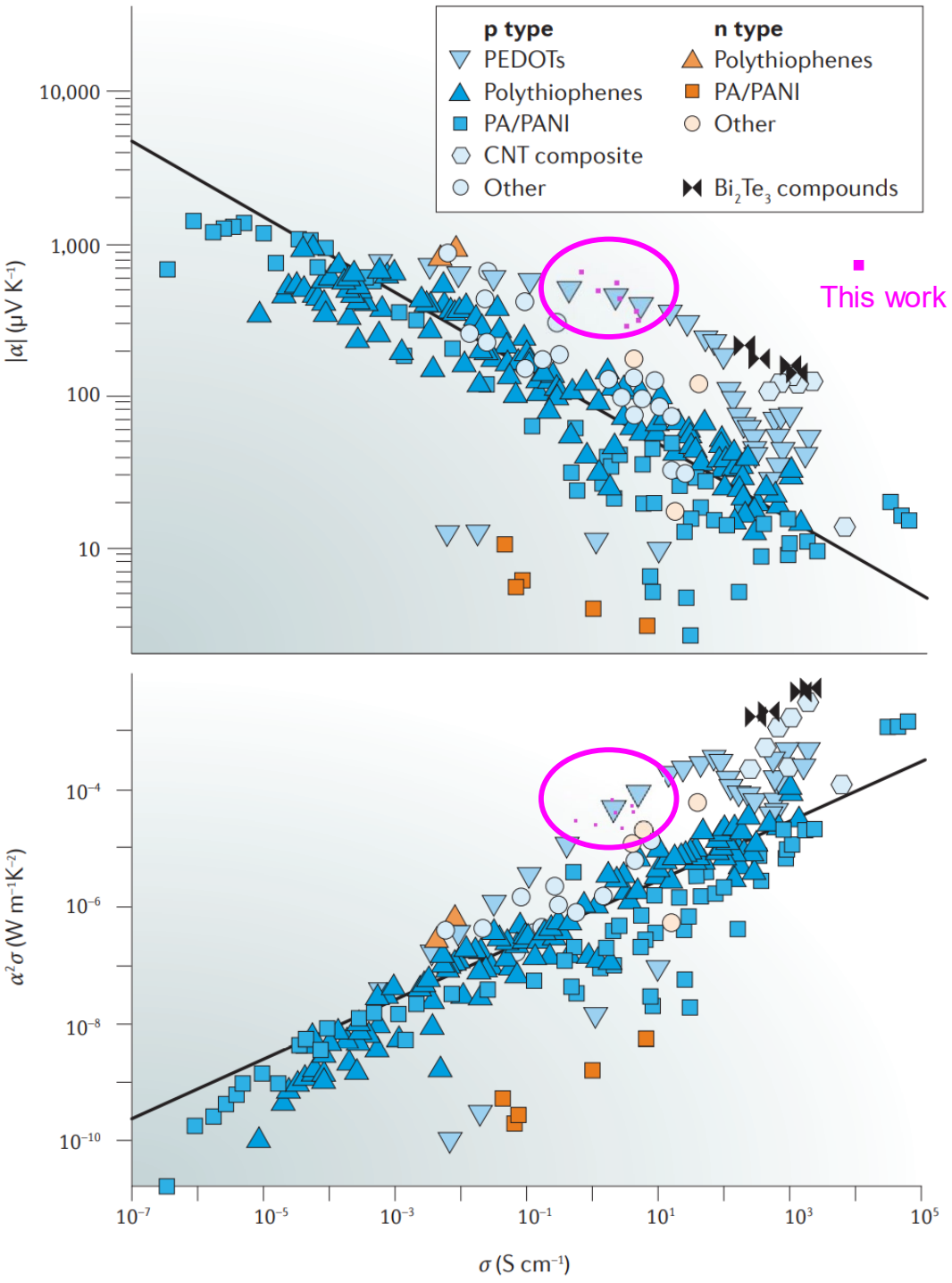

Figure 6. Seebeck coefficient (α; top) and power factor ($\alpha 2\sigma$; bottom) as functions of conductivity (σ) for a range of doped organic thermoelectric (OTE) polymers and composites summarized by Boris Russ et al.[3] with data from the present work superimposed. Reprinted by permission from Nature/Springer/Palgrave) B. Russ, A. Glaudell, J. J. Urban, M. L. Chabinyc, R. A. Segalman, *Nat. Rev. Mater.* **2016**, *1*, 16050. Copyright 2016.

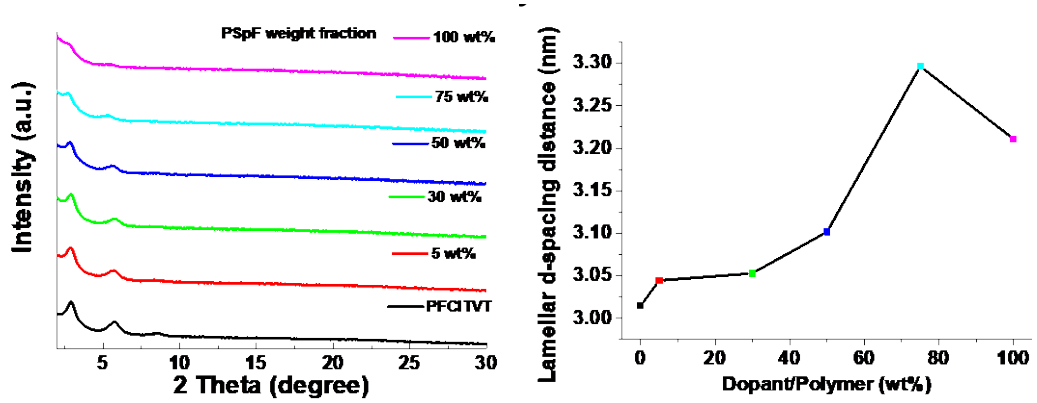

Figure 7. (a) Out-of-plane GIXRD diagrams of pristine and doped polymer films which are prepared similarly to the thermoelectric devices. (b) Lamellar *d*-spacing distances of polymers doped with various weight fractions of dopant.

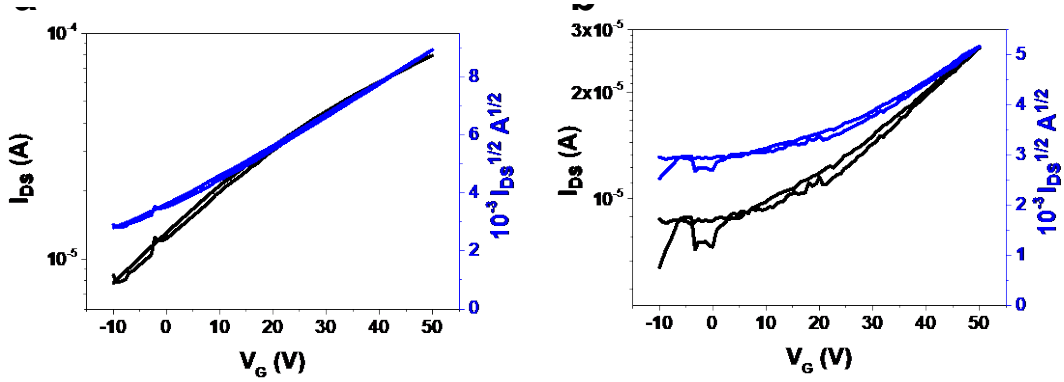

Figure 8. Transfer curves of OFETs of (a) 2 wt% and (b) 10 wt% PSpF doped polymer thin films.

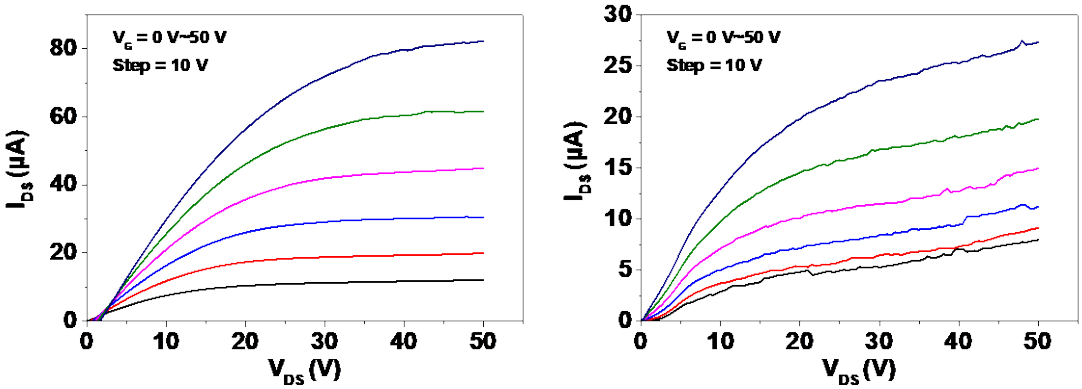

Figure 9. Output curves of OFETs of (a) 2 wt% and (b) 10 wt% PSpF doped polymer thin films.

Table 2. OFET device performance of the pristine and doped polymers.

Polymer films	μ_e ($cm^2 V^{-1} s^{-1}$)	V_T (V)	I_{on}/I_{off}
PFClTVT	0.24±0.04	35-40	500-1000
1 wt% PSpF	0.81±0.05	-7--21	80-100
2 wt% PSpF	0.37±0.01	-25	10-15
10 wt% PSpF	0.13±0.05	-3--22	3-400

Table 3. EDS element analysis of pristine PFClTVT film in different spots.

Element	Spot 1 Atomic %	Spot 2 Atomic %	Spot 3 Atomic %	Spot 4 Atomic %	Spot 5 Atomic %	Spot 6 Atomic %
C K	52.54	52.46	61.49	70.23	53.08	53.06
O K	9.58	9.51	12.22	11.05	9.54	9.15
F K	0.14	0.18	0.5	0.32	0.17	0.17
Si K	35.77	35.68	23.26	13.59	35.26	35.37
S K	0.56	0.59	0.58	1.57	0.55	0.63
Cl K	0.56	0.66	0.83	1.59	0.53	0.63
Cr K	0.85	0.92	61.49	1.65	0.86	0.99

Table 4. EDS element analysis of 5 wt% PSpF doped PFClTVT film in different spots (Spot 6 is dust).

Element	Spot 1 Atomic %	Spot 2 Atomic %	Spot 3 Atomic %	Spot 4 Atomic %	Spot 5 Atomic %	Spot 7 Atomic %	Spot 8 Atomic %
C K	74.53	77.61	75.04	73.45	74.61	73.64	72.96
O K	10.61	7.89	7.27	6.08	8.27	5.9	6.22
F K	2	1.25	0.63	0.96	1.61	0.89	1.03
Br L	0.2	0.27	0.27	0.22	0.21	0.22	0.24
Si K	2.75	7.66	11.72	14.46	7.64	14.29	14.89
S K	2.37	2.01	1.92	1.79	2.34	1.88	1.73
Cl K	2.54	1.59	1.7	1.92	2.47	1.86	1.79
Ag L	3.53	0.19	0.24	0.11	1.3	0.13	0.1
Cr K	1.47	1.53	1.22	1.01	1.55	1.19	1.04

Table 5. EDS element analysis of 50 wt% PSpF doped PFClTVT film in different spots (Spot 3 is dust).

Element	Spot 1 Atomic %	Spot 2 Atomic %	Spot 4 Atomic %	Spot 5 Atomic %	Spot 6 Atomic %	Spot 7 Atomic %	Spot 8 Atomic %
C K	76.32	78.87	74.09	77.8	78.01	76.7	77.96
O K	10.5	5.27	13.48	6.39	7.95	9.3	5.48
F K	0.56	0.92	0.97	1	1.03	0.82	0.78
Br L	0.24	0.32	0.32	0.33	0.36	0.35	0.37
Si K	7.94	9.64	6.03	9.46	6.98	7.87	10.47
S K	1.21	1.55	1.24	1.62	1.61	1.36	1.62
Cl K	1.57	1.74	1.83	1.67	2.13	1.7	1.73
Ag L	0.18	0.3	0.26	0.32	0.39	0.24	0.31
Cr K	1.47	1.39	1.8	1.4	1.55	1.65	1.28

Table 6. EDS element analysis of pristine PSpF film in different spots (Spot 3 is dust).

Element	Spot 1 Atomic %	Spot 2 Atomic %	Spot 3 Atomic %	Spot 4 Atomic %	Spot 5 Atomic %
C K	90.19	89.23	90.51	37.65	86.53
O K	3.03	2.6	2.8	0	5.56
Br L	1.24	1.02	1.16	0.04	0.93
Si K	0.2	2.08	0.38	56.77	2.04
S K	0.21	0.24	0.28	0.05	0.19
Cl K	1.18	1.12	1.2	0.39	1
Ag L	1.68	1.36	1.37	0.52	1.24
Cr K	2.26	2.34	2.31	4.57	2.5

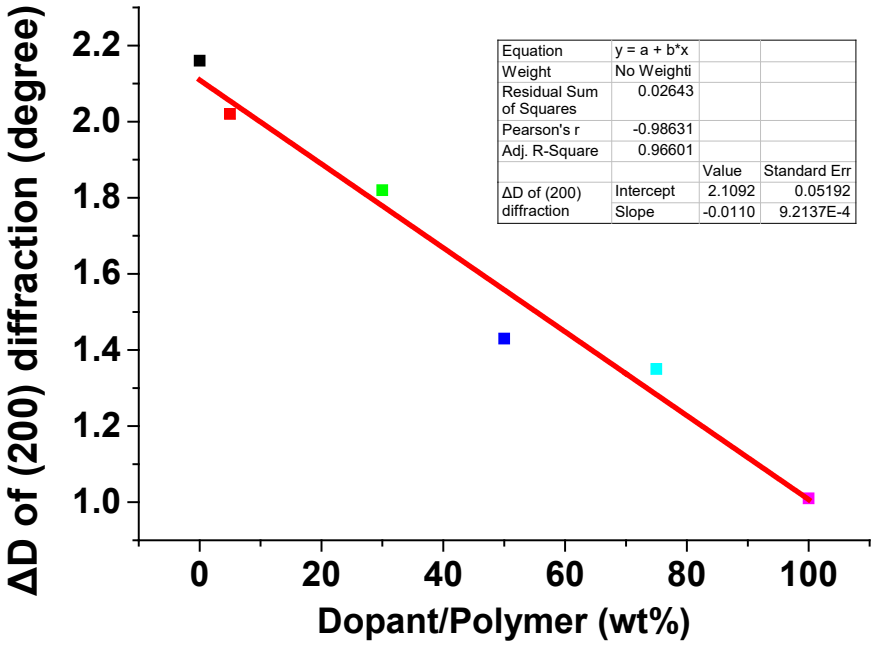

Figure 10. Linewidth of the (200) peak of pristine and doped thin films.

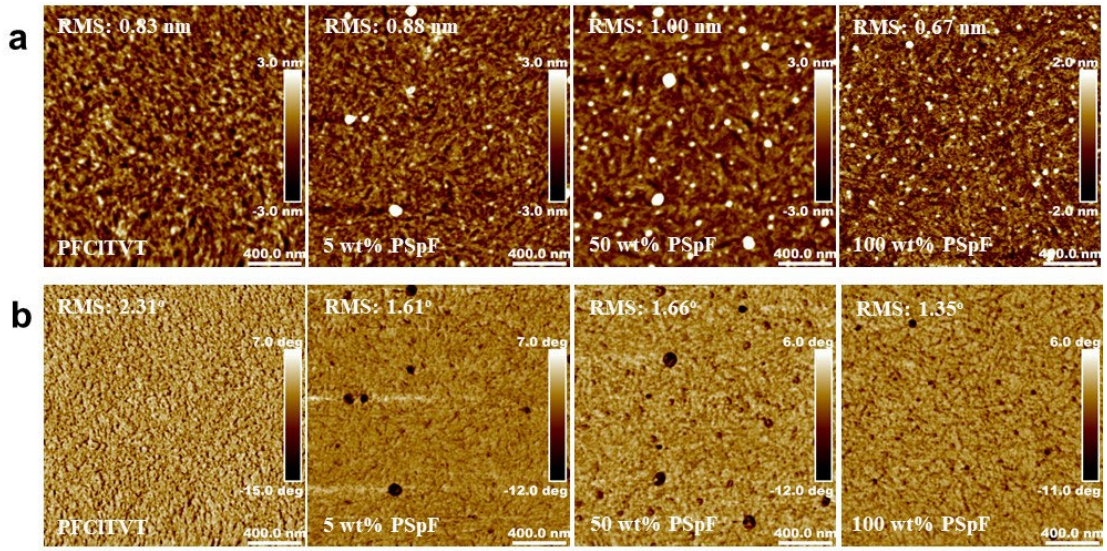

Figure 11. AFM (a) height images and (b) phase images of pristine and PSpF doped polymer thin films.

References

[1] J. Han, H. Fan, Q. Zhang, Q. Hu, T. P. Russell, H. E. Katz, *Adv. Funct. Mater.* **2021**, *31*, 2005901.

[2] X. Zhao, D. Madan, Y. Cheng, J. Zhou, H. Li, S. M. Thon, A. E. Bragg, M. E. DeCoster, P. E. Hopkins, H. E. Katz, *Adv. Mater.* **2017**, *29*, 1606921.

[3] B. Russ, A. Glaudell, J. J. Urban, M. L. Chabinyc, R. A. Segalman, *Nat. Rev. Mater.* **2016**, *1*, 16050.